Materials Science in Semiconductor Processing 169 (2024) 107912

Contents lists available at ScienceDirect

Materials Science in Semiconductor Processing

journal homepage: www.elsevier.com/locate/mssp

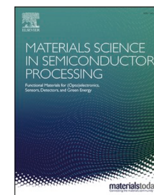

Preparation of high light-trapping β-Ga_2O_3 nanorod films via thermal oxidation of GaAs and metal-organic chemical vapor deposition

Wei Chen [a,b], Teng Jiao [a], Peiran Chen [a], Xinming Dang [a], Yu Han [a], Han Yu [a], Xin Dong [a,*], Yuantao Zhang [a], Baolin Zhang [a]

[a] State Key Laboratory of Integrated Optoelectronics, College of Electronic Science & Engineering, Jilin University, Changchun, 130012, China
[b] State Key Laboratory of Luminescence and Applications, Changchun Institute of Optics, Fine Mechanics and Physics, Chinese Academy of Sciences, Changchun, 130012, China

ARTICLE INFO

Keywords:
β-Ga_2O_3
Nanorod
Thermal oxidation
MOCVD

ABSTRACT

Monoclinic gallium oxide (β-Ga_2O_3) has attracted wide attention due to its low-cost single crystal and excellent optoelectronic properties. However, the low specific surface area and high defect density of β-Ga_2O_3 thin films result in weak light-matter interaction and poor crystal quality, seriously hindering their applications. In this article, the growth of high light-trapping β-Ga_2O_3 nanorod (NR) film on GaAs substrates by metal-organic chemical vapor deposition (MOCVD) is demonstrated. The GaAs substrates were pre-treated by thermal oxidation (TO) to produce a β-Ga_2O_3 seed layer. The effect of MOCVD growth conditions on the morphology of β-Ga_2O_3 NR films is investigated. The growth mechanism of β-Ga_2O_3 NR films is studied in detail. X-ray diffraction, Raman, and photoluminescence were employed to study the crystal and optical properties of β-Ga_2O_3 NR films. A significant light-trapping effect with a 40 % reduction in optical reflectance at the wavelength of 254 nm is observed. The results show that the β-Ga_2O_3 NR films exhibit strong light-matter interaction and have potential in optoelectronic applications.

1. Introduction

Due to the ultra-wide bandgap of 4.9 eV, and superior thermal and chemical stability, β-Ga_2O_3 is considered an ideal candidate for power devices and solar-blind ultraviolet (SBUV) detection [1–5]. Various morphologies of β-Ga_2O_3 have been developed, including single crystals [6,7], thin films [8–11], nanostructures [12,13], and other structures. Low-dimensional nanostructures of NRs, in particular, have attracted significant attention due to their lattice strain relaxation [14,15], strong light-matter interaction [16], and carrier transport regulation [17]. These nano-features are expected to explore the potential applications of β-Ga_2O_3 in gas sensing, SBUV detection, and field emission devices. For example, Chu et al. reported a β-Ga_2O_3 NR NO_2 gas sensor with a responsivity of 34.2 % to a low NO_2 concentration of 100 ppb [18]. Wei et al. fabricated a β-Ga_2O_3 NR-based SBUV photodetector, achieving the dark current of 2.04×10^{-9} at 1 V [19]. A field emission device based on β-Ga_2O_3 NRs with a threshold electric field of 5.6 V/m, and a geometrical field enhancement factor of 3786 was reported [20].

Currently, several methods have been adopted to synthesize β-Ga_2O_3 nanostructures, including physical vapor deposition [21], chemical vapor synthesis [22,23], and solution-based techniques [24]. However, these approaches involve metal catalysts or dry etching, resulting the undesirable contamination or lattice damage. Whereas, MOCVD is a modern epitaxy technology with the unique advantages of high film uniformity and parameter adjustability. However, the reports on the growth of β-Ga_2O_3 NRs by MOCVD are still limited. In addition, to prepare high crystalline β-Ga_2O_3 NR films, several problems still need to be solved, such as avoiding the involvement of metal catalysts and the influence of MOCVD parameters on the film characteristics.

In this paper, we report a novel approach for synthesizing β-Ga_2O_3 NR films on intrinsic GaAs (i-GaAs) (100) substrates by integrating TO and MOCVD. The influence of MOCVD growth temperature and gas-phase VI/III ratio on structural, optical, and crystal properties of the fabricated samples were investigated. Scanning electron microscope (SEM), X-ray diffraction (XRD), photoluminescence (PL), and Raman analyses were carried out to study the β-Ga_2O_3 NR films. The formation mechanism of β-Ga_2O_3 NRs during the MOCVD process was studied in detail. The optical trapping effect of β-Ga_2O_3 NR films was examined by

* Corresponding author.
E-mail address: dongx@jlu.edu.cn (X. Dong).

https://doi.org/10.1016/j.mssp.2023.107912
Received 14 July 2023; Received in revised form 21 September 2023; Accepted 15 October 2023
Available online 1 November 2023
1369-8001/© 2023 Elsevier Ltd. All rights reserved.

reflection spectrum.

2. Experimental

2.1. Preparation of β-Ga_2O_3 NR films

To enhance the growth anisotropy of MOCVD, a β-Ga_2O_3 nanowire (NW) seed layer was introduced. The β-Ga_2O_3 seed layer was prepared by TO of i-GaAs substrates. The detail of the TO procedure was described in our previous study [25]. Before the TO process, sequential ultrasonic cleaning was performed on the i-GaAs substrates in acetone, ethanol, and deionized water for 5 min to remove the contamination on the i-GaAs surface. The TO reaction was performed for 30 min under a pressure of 1 bar using O_2 (5 N) as reaction gases and N_2 (5 N) for dilution. It is found that the β-Ga_2O_3 seed layer produced by i-GaAs substrates exhibits sparser β-Ga_2O_3 NWs than those obtained from *p*-GaAs [25]. This morphology difference may be derived from the lattice difference caused by doping. Therefore, the TO process was carried out at a lower temperature of 850 °C. Furthermore, the impact of the O_2 flow rate on the formation of the β-Ga_2O_3 seed layer was investigated by SEM. As shown in Fig. 1, the surface of the produced β-Ga_2O_3 seed layers exhibits nanoparticle features at a low O_2 flow rate. The nanoparticles transform into NW structures and become denser with increasing O_2 flow rate. After that, the surface turns island-like when the O_2 flow rate exceeds 0.3 L/min. Accordingly, the O_2 flow rate of the TO process was chosen to be 0.2 L/min in the following experiments. And the sample with an O_2 flow rate of 0.2 L/min was named S1 for further discussion.

The β-Ga_2O_3 film was grown on the β-Ga_2O_3 seed layer by MOCVD. The O_2 (5 N) and trimethylgallium (TMGa) were used as the O and Ga sources, respectively. The Ga source was introduced into the chamber by blowing argon (5 N) into the TMGa cylinder. The chamber is designed with a close-coupled showerhead and a graphite tray to create a consistent gas flow and temperature field. The adopted MOCVD growth parameters are shown in Table 1, four samples of S2 to S5 were prepared to investigate the effects of growth temperature and the gas-phase VI/III ratio on the morphology and physical properties of β-Ga_2O_3 NR films. The Ga flow rate is controlled at a low level to suppress the coalescence of the nucleus on the polycrystalline surface of the NW seed layer and reduce the growth rate, thereby promoting the growth of β-Ga_2O_3 NRs [26]. The vapor phase VI/III ratio was regulated by adjusting the Ga flow rate from 5 to 10 sccm, and the growth pressure and O_2 flow rate were kept constant at 20 mbar and 400 sccm, respectively, for all samples.

2.2. Characterization methods

The morphology of β-Ga_2O_3 NR films was examined using SEM (JSM-7610, JOEL). The Raman spectra were obtained through a laser confocal Raman microscope (LabRAM HR Evolution, Horiba) utilizing the 532 nm laser excitation. The crystal structure investigation was conducted via XRD (SmartLabSE, Rigaku). The grazing incidence configuration, with an incident angle of approximately 5°, was employed to scrutinize the crystal characteristics of β-Ga_2O_3 NRs on the film's surface. PL spectra of β-Ga_2O_3 NR films were measured through a spectrometer (iHR550, Horiba) after the stimulation with a YAG laser at a wavelength of 235 nm. The reflection spectrum was characterized via a spectrophotometer (UV3600, Shimadzu) equipped with an integrating sphere. All experiments were carried out at room temperature.

Table 1
The adopted MOCVD growth parameters.

Sample	Growth temperature (°C)	Ga flow rate (sccm)	Vapor phase VI/III ratio (10^3)
S2	750	10	11.2
S3	750	5	22.4
S4	700	10	11.2
S5	700	5	22.4

3. Results and discussion

3.1. Morphology analysis

To evaluate the influence of MOCVD growth conditions on β-Ga_2O_3 NR films, we characterized the morphology and size of the samples. As shown in Fig. 2, the top view and 45° inclined SEM images show all samples display dense and rod-like nanostructures on their surface, demonstrating the successful preparation of β-Ga_2O_3 NR film. In terms of growth temperature, the SEM images of S2 and S3 (Fig. 2 (b) and (c)) reveal that β-Ga_2O_3 NRs prepared at 750 °C exhibit rough sidewalls and dense grain attachments. In contrast, β-Ga_2O_3 NRs in S4 and S5 obtained at 700 °C (Fig. 2 (d) and (e)), are smoother compared to those grown at higher growth temperatures. In addition, it is found that the vapor phase VI/III ratio mainly affects the diameter of β-Ga_2O_3 NRs. In Fig. 2 (k), the average diameter of β-Ga_2O_3 NRs prepared at the same growth temperature remains relatively consistent. The average diameter of β-Ga_2O_3 NRs increases from approximately 270 nm–585 nm when the vapor phase VI/III ratio is reduced from 22.4 × 10^3 to 11.2 × 10^3. Moreover, the 45° perspective views depicted in Fig. 2 (g)–(j) reveal that the β-Ga_2O_3 NRs in all samples are approximately 2 μm in length, indicating a growth saturation in the axial direction. In Fig. 2 (d), the β-Ga_2O_3 NRs exhibit a rounded morphology, whereas those in S5 (Fig. 2 (e), (j)) show a cubic shape with well-defined edges between different crystal faces and a clear boundary between the β-Ga_2O_3 layer and NRs, indicating a better crystal quality. These findings are discussed further in the following section.

3.2. Mechanism analysis

The Ga supersaturation (σ_{Ga}) is taken into consideration to analyze the growth of the β-Ga_2O_3 NRs:

$$\text{Log}(P^0_{Ga}) = A + \frac{B}{T} + C \times \text{Log}(T) \tag{1}$$

$$P_{Ga} = P\frac{F_{Ga}}{F} \tag{2}$$

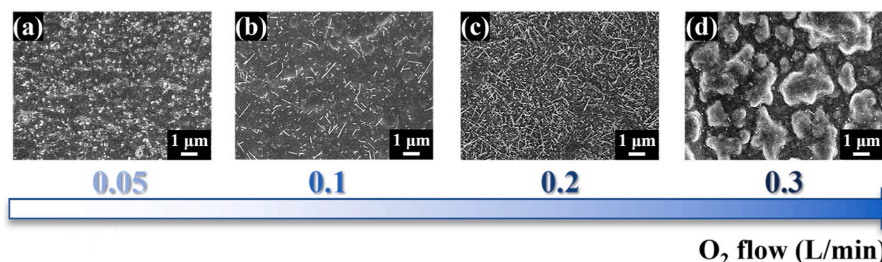

Fig. 1. Top view SEM images of samples prepared by TO of i-GaAs at different O_2 flow rates of 0.05, 0.1, 0.2, and 0.3 L/min.

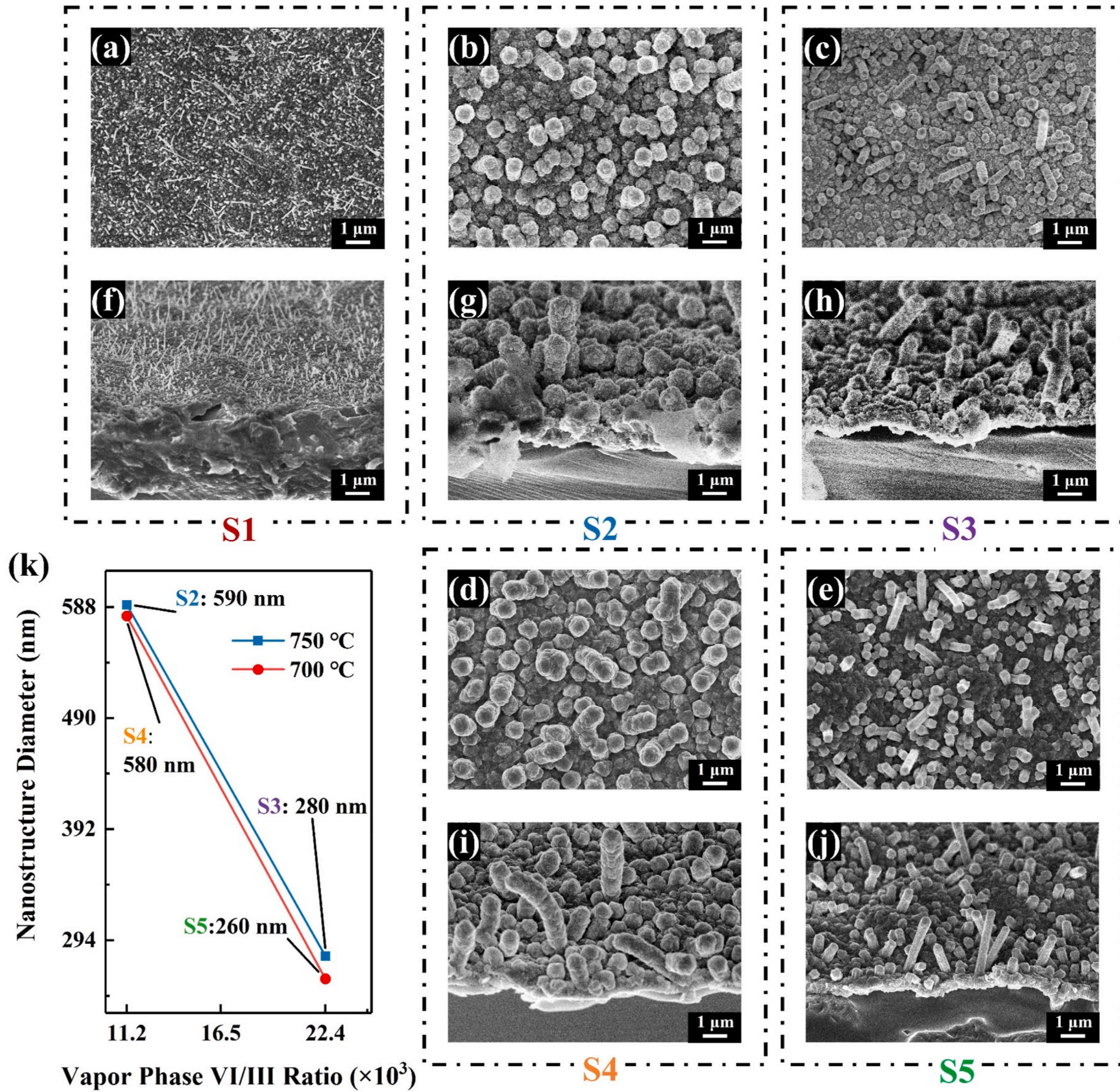

Fig. 2. (a)–(j) are the SEM images of S1 to S5, where (a) to (e) are the top views, and (e) to (h) are the 45° inclined views. (k) the average diameter statistics of S2 to S5.

$$\sigma = \frac{P_{Ga}^{0} - P_{Ga}}{P_{Ga}} \quad (3)$$

where P_{Ga}^{0} denotes Ga vapor pressure at the gas-solid interface, the *A*, *B,* and *C* are thermodynamic constants with values of 6.754, −13984, and −0.3413, respectively [27]. *T* is the growth temperature. P_{Ga} is the gas partial pressure of Ga in the MOCVD chamber, and *P* is the growth pressure of 20 mbar. *F* represents the total gas flow rate of 3.4 slm, while F_{Ga} represents the Ga flow rate. It is worth noting that the Ar flow rate is considered the Ga flow rate because Ar carries the Ga precursor from the TMGa cylinder. The calculated Ga supersaturation is shown in Fig. 4. It can be observed that the σ_{Ga} decreases as the Ga flow rate decreases in the growth temperature range of 700–750 °C. This trend weakens as the growth temperature increases. Furthermore, the σ_{Ga} decreases with increasing growth temperature. Additionally, within the range of MOCVD growth parameters adopted in the experiment, the σ_{Ga} keeps at a low level below 100. The low σ_{Ga} effectively reduces the lateral growth caused by the coalescence and merging of the nucleus, thereby promoting axial growth.

Based on the above analysis, the growth mechanism and the influence of MOCVD growth parameters on β-Ga_2O_3 NR films are further studied. Due to the catalyst-free characteristic, it is suitable to utilize the gas-solid mechanism to analyze the growth behavior of β-Ga_2O_3 NRs [28]. The β-Ga_2O_3 NWs formed on i-GaAs surfaces through TO pre-treatment can be considered seed crystals. These seed crystals serve as preferential nucleation sites for Ga atoms during the MOCVD process. This anisotropic surface state of the NW seed layer facilitates the migration of reactant atoms toward the top face of the NWs, thereby promoting a transition in the growth mode towards anisotropic growth. The top surface of self-nucleated, catalyst-free β-Ga_2O_3 NRs grown by MOCVD can be conceptualized as a singular terrace enclosed by an infinitely high cubic-shaped step boundary [29]. This boundary creates an Ehrlich-Schwöbel barrier that restricts the downward diffusion of Ga [30]. The Ga atoms deposited on the substrate and the sidewalls of the NRs diffuse and are trapped at the step of the top surface of the β-Ga_2O_3 NR. This leads to nucleation and subsequent elongation growth of the β-Ga_2O_3 NRs. It should be noted that the low Ga supersaturation and gas phase VI/III are favorable for the diffusion process of Ga atoms on the substrate and β-Ga_2O_3 NR sidewall regions. As illustrated in Fig. 3, a layered growth model is employed to analyze the growth process of the β-Ga_2O_3 NRs. The reactant atoms presented on the β-Ga_2O_3 NW top and

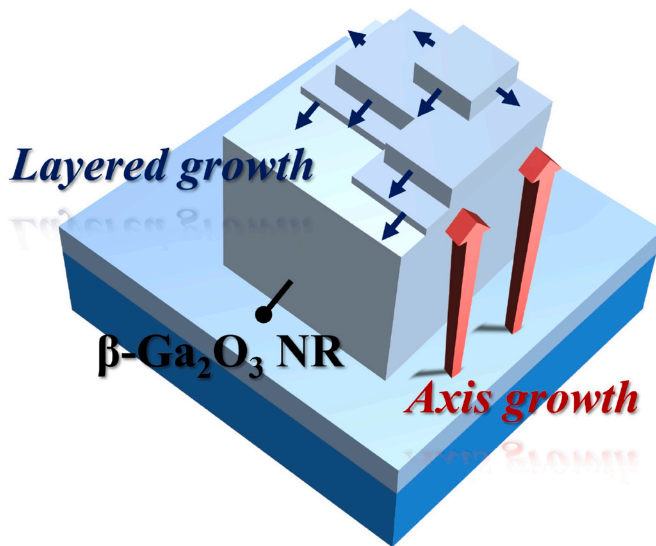

Fig. 3. The illustration of the axis growth mode of β-Ga_2O_3 NRs.

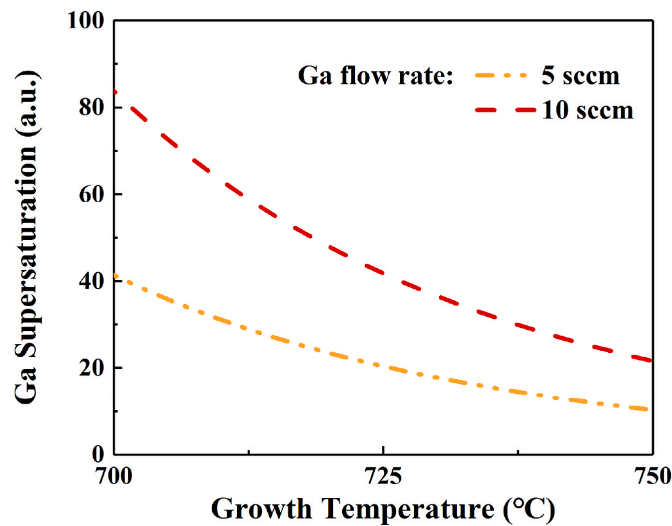

Fig. 4. Calculated Ga supersaturation in the MOCVD process.

those that migrate from the seed layer surface are constrained by the step barrier. Due to the low Ga supersaturation maintained in the MOCVD system, the reactant atoms undergo nucleation in a few- or single-mode, subsequently resulting in the layered growth of β-Ga_2O_3. Once a layer is fully formed, the β-Ga_2O_3 NR growth proceeds to the next layer.

At this state of low σ_{Ga}, the growth of β-Ga_2O_3 primarily manifests as layered growth in the top surface region of nanostructures. The β-Ga_2O_3 NR growth rate can be described by the following equation [31]:

$$v = \left(\left(\frac{\sqrt{b}\sigma_{Ga}}{kT} \right) - \frac{\sqrt{b}4\Omega\alpha_{vs}}{kTd} \right)^2 \tag{4}$$

where b is the kinematic crystallization coefficient, k, and T are the Boltzmann constant and growth temperature. Ω denotes the atomic volume of reactants, d is the diameter of NRs, and α_{vs} represents the average surface energy density of the NRs. Equation (4) reveals that the axial growth rate of β-Ga_2O_3 NRs decreases as the growth temperature increases. The weakening of axial growth leads to more reactant atoms bonding with the β-Ga_2O_3 NR sidewalls and forming the crystal grains. In terms of the gas-phase VI/III ratio, the decrease of the gas-phase VI/III ratio (increasing the Ga flow rate) transforms the β-Ga_2O_3 NRs' growth from few- or single-mode to multi-mode nucleation. The following equation governs the growth rate at the multi-mode nucleation stage [32]:

$$v = \left(\pi V^2 J / 3\right)^{1/3} \tag{5}$$

where J is the nucleation rate, and V denotes the growth rate of the crystal nucleus. The reduction of the gas-phase VI/III ratio increases the nucleation rate. This phenomenon results in the saturation of the growth rate at the top of the β-Ga_2O_3 NRs, inhibiting the anisotropic growth and gradually shifting towards lateral growth, leading to an increase in the diameter of the β-Ga_2O_3 NRs.

3.3. Material property analysis

The structural properties of β-Ga_2O_3 NR films were investigated. In the Raman spectra of Fig. 5, all samples exhibit two patterns, the peak at 200 cm^{-1} is the $A_g^{(3)}$ pattern of β-Ga_2O_3 [33], and the other peak at 258 cm^{-1} is contributed by $A_g^{(1)}$ of As [34]. For S1, the LO characteristic peak located at 290 cm^{-1} belonging to GaAs is also observed [35]. The weak peaks observed at 346 cm^{-1} and 416 cm^{-1} in Raman spectra of S2 to S5 are attributed to $A_g^{(5)}$ and $A_g^{(6)}$ of β-Ga_2O_3, respectively. The Raman measurements prove that pure β-Ga_2O_3 is formed. The residue of arsenic may result from the TO process. However, from S2 to S5, a decrease in the peak intensity related to arsenic is observed, indicating that further heat treatment might alleviate the problem of arsenic residue.

The grazing incidence XRD was adopted to study the crystal properties of β-Ga_2O_3 NR films. In the XRD 2θ spectra depicted in Fig. 6 (a), all samples exhibit the same diffraction peaks of (400), (12), and (03) crystal planes (JCPDS PDF card No. 43–1012, space group $C2/m$). The shoulder peak near the (400) diffraction peak of β-Ga_2O_3 belongs to the diffraction peak of the GaAs (200) crystal plane, forming by the leakage of the GIXRD signal into the i-GaAs substrate. The preferential orientation of the (400) crystal plane is consistent with previously reported results [8]. The peak intensities of the β-Ga_2O_3 XRD patterns increase with morphological improvement for all samples. To further study the crystal properties of β-Ga_2O_3 NR films, the full width at half maximum (FWHM) of the highest diffraction peak ((400) crystal plane) of β-Ga_2O_3 was calculated. In Fig. 6 (b), the β-Ga_2O_3 NR film (S2) exhibits a slight degradation in the FWHM compared to the β-Ga_2O_3 seed layer (S1). Furthermore, the FWHM gradually decreases with the optimization of growth conditions, and the FWHM of S5 is reduced to approximately 0.455. The above observations indicate that the crystal quality of the β-Ga_2O_3 NR films is improved compared to the seed layer, and there is a positive correlation between the crystal quality and the morphology. Under appropriate MOCVD process parameters, the reactant atoms can migrate to their optimal sites to form β-Ga_2O_3 with high crystal quality,

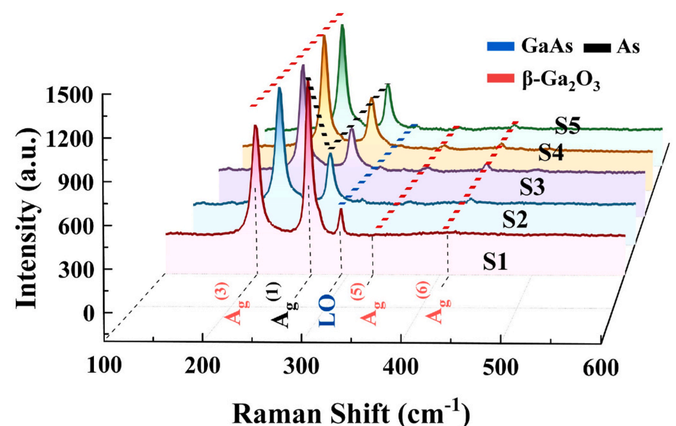

Fig. 5. Raman patterns of S1 to S5.

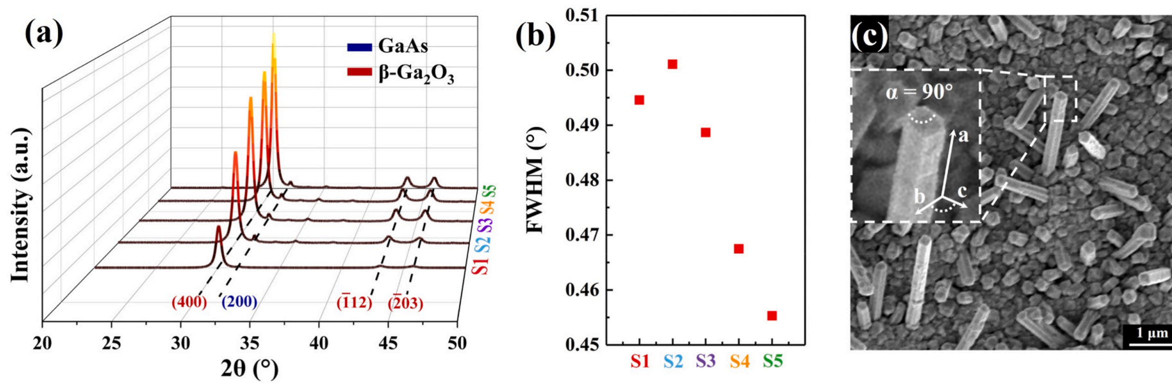

Fig. 6. (a) XRD 2θ spectra, (b) FWHM of the (400) diffraction peak of β-Ga_2O_3 for samples S1 to S5. (c) the magnified SEM image of S5.

whereas rapid lateral growth results in a surge of lattice defects, thus deteriorating the crystal quality. Fig. 6 (c) provides a magnified SEM image of a single β-Ga_2O_3 NR in S5. This image evidences that the square tip of the β-Ga_2O_3 NR has a rectangular shape and an edge length of approximately 260 nm, with a feature angle α of approximately 90°. The α is consistent with the angle between the (010) and (001) crystal planes of the β-Ga_2O_3 unit cell, indicating that the growth of the β-Ga_2O_3 NRs is along the a-axis of the (400) crystal plane.

The PL characteristics of β-Ga_2O_3 NR films were investigated. As shown in Fig. 7, all samples show two PL peaks. The ultraviolet emission located at 360 nm is derived from the radiation recombination of self-trapped excitons [36], and the blue emission at about 410 nm is excited by the donor-acceptor pair recombination [37]. The PL peaks of S2 to S5 are significantly increased compared to the β-Ga_2O_3 seed layer (S1). The increase in the intensity of the PL and XRD peaks confirms the crystal quality improvement, which is consistent with the morphology analysis.

To reduce the residue of arsenic, the sample of S5 was annealed at 500 °C in an N_2 atmosphere for 30 min. The energy dispersive spectrometer (EDS) was adopted to study the impact of annealing on the elemental composition. The EDS spectra and elemental distribution maps are shown in Fig. 8. It can be seen that the characteristic peak of arsenic element shows in the EDS spectrum of the unannealed sample (Fig. 8 (a)) with an arsenic content of 2.4 %. However, after annealing, the arsenic characteristic peak disappears (Fig. 8 (b)) and the arsenic content reduces to 0.21 %. Considering that the energy of EDS can penetrate the GaAs substrate, the actual arsenic content in the annealed sample is even lower. Besides, it can be observed from the elemental distribution map of Fig. 8 (c) and (d) that compared to the distribution of O (which forms the β-Ga_2O_3 NRs), the distribution of arsenic element is uniform. This result suggests that the arsenic element is not distributed in the β-Ga_2O_3 NRs but rather in the GaAs substrate or seed layer. The results of the EDS measurement confirm that the annealing process can effectively reduce the residual arsenic content in the β-Ga_2O_3 NR film.

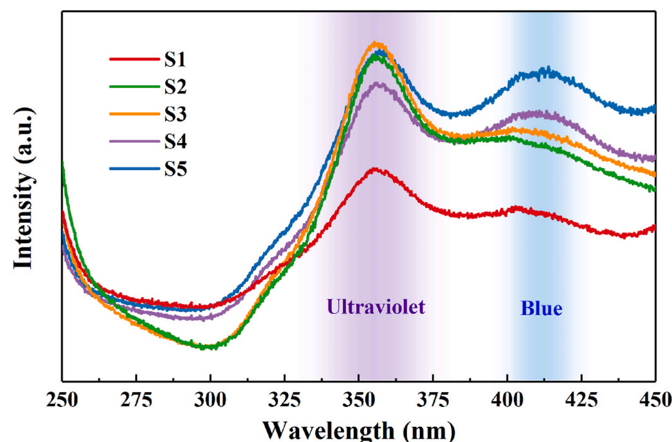

Fig. 7. PL spectra of S1 to S5.

3.4. *Light-trapping effect*

The light-trapping effect of the β-Ga_2O_3 NR film was studied. The optical transmission of β-Ga_2O_3 thin film and NR film was simulated by the finite element method. A single period of the S5 cross-section was constructed. The left and right sides of the model were defined as the Floquent boundary to conform to the infinite periodic structure. The β-Ga_2O_3 thin film was defined with a 400 nm-thick β-Ga_2O_3 layer. Fig. 9 presents the simulation results of the optical transmittance spectra (absorption A and reflectance R) of two kinds of β-Ga_2O_3 films. As shown in Fig. 9 (a), under an incident wavelength of 254 nm (SBUV), the β-Ga_2O_3 NR film displays optimal values for R and A at a period of 750 nm. These are 85.6 % and 13.8 % higher than the corresponding values of β-Ga_2O_3 thin film. Moreover, it is observed that the R and A of the NR film are consistently higher than those of the thin film across all periods. This light-trapping phenomenon can be attributed to the strong optical oscillation occurring within the individual β-Ga_2O_3 NRs, as demonstrated in the inset of Fig. 9 (a). The β-Ga_2O_3 NR film shows strong light-trapping within a broad optical band compared to the thin film, as shown in Fig. 9 (b). In Fig. 9 (c), the R of the β-Ga_2O_3 NR film remains stable initially as the incident angle increases and subsequently increases after reaching 40°. Furthermore, the corresponding trend of A is observed to parallel that of R. The average values of R and A of β-Ga_2O_3 NR films are 55.4 % and 18.5 % higher than those of thin films.

The reflectance spectra of both β-Ga_2O_3 thin film and NR film were further studied using a spectrophotometer. The preparation of the β-Ga_2O_3 thin film also adopts the MOCVD technique and (100) oriented i-GaAs substrate. XRD measurement indicates that the β-Ga_2O_3 thin film exhibits a polycrystalline state. The thickness of the β-Ga_2O_3 thin film is 466 nm measured by the ellipsometer. The details of the material properties of β-Ga_2O_3 thin films are attached in the Supporting Information. Fig. 10 shows that the measured optical reflectance spectrum is consistent with the trend predicted by simulation results in Fig. 9 (b). In addition, compared to their thin film counterparts, β-Ga_2O_3 NR film exhibits excellent light reflection suppression capabilities over a broad spectral range from ultraviolet to near-infrared wavelengths. The average reflectance of the β-Ga_2O_3 NR film is found to be less than 0.1, indicating an efficient reduction of specular reflectance. In particular, at a wavelength of 254 nm (within the SBUV band), the optical reflectance of the β-Ga_2O_3 NR film is approximately 0.05, which is 40 % lower than that of the β-Ga_2O_3 thin film. This indicates that the β-Ga_2O_3 NR film shows promise in SBUV light sensing.

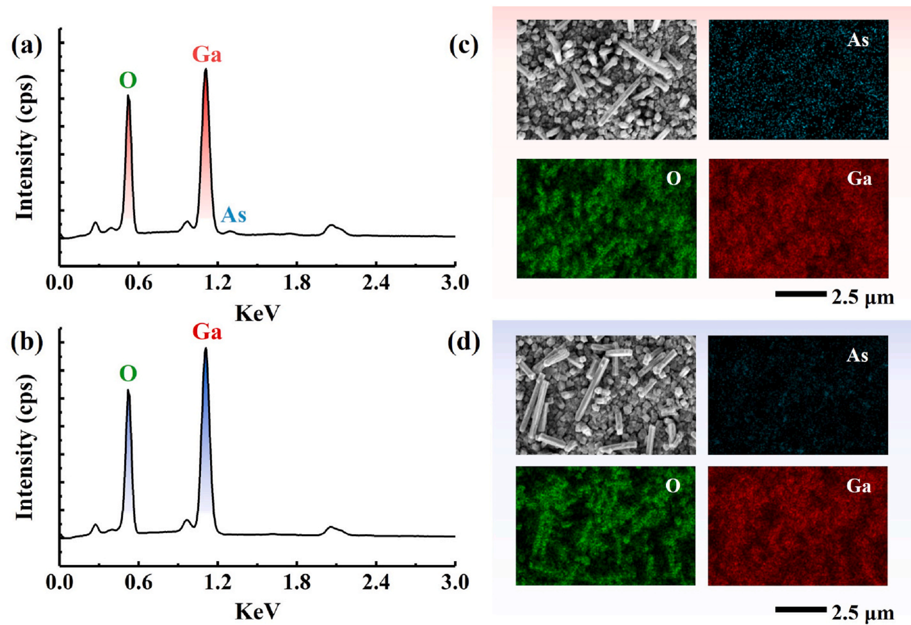

Fig. 8. (a) and (c) are the EDS spectrum and elemental distribution map of the unannealed sample, respectively. (b) and (d) are the EDS spectrum and elemental distribution map of the annealed sample, respectively.

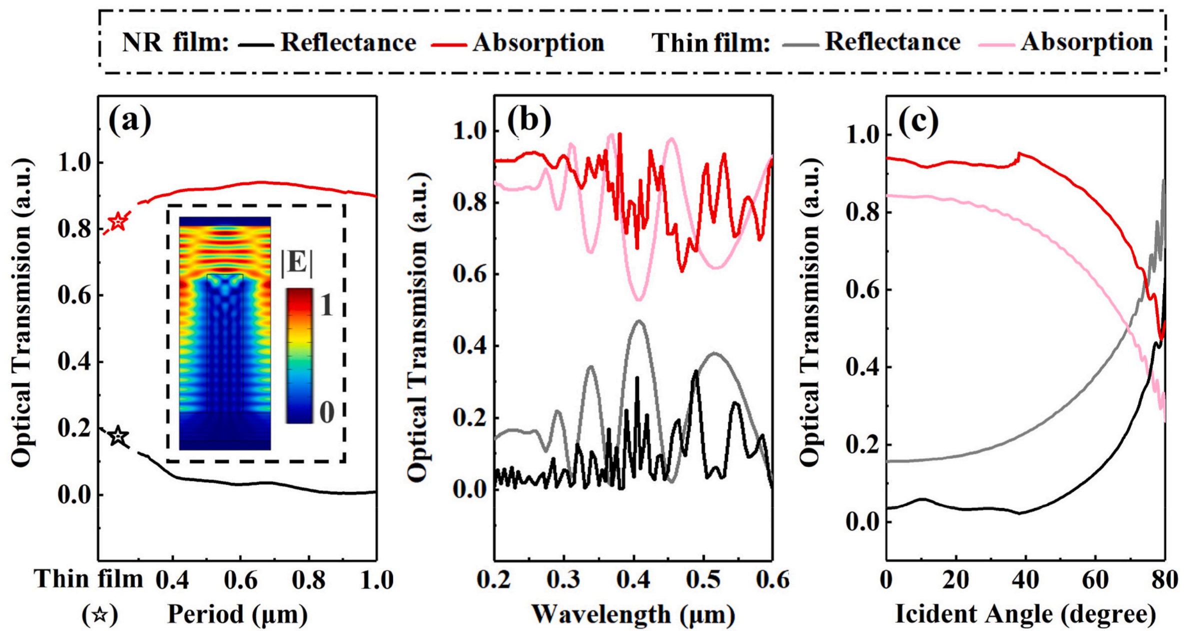

Fig. 9. (a)–(c) are optical transmission spectra versus period, wavelength, and incident angle, respectively. The inset in (a) is the light field distribution of a unit of the simulated structure with a β-Ga_2O_3 NR.

4. Conclusion

In summary, we demonstrate the synthesis of β-Ga_2O_3 NR films via a two-step process involving TO of i-GaAs and MOCVD. The effects of the gas-phase VI/III ratio and growth temperature of MOCVD on the characteristics of the β-Ga_2O_3 NR films are systematically investigated. The results show that reducing the MOCVD growth temperature and Ga flow rate led to axial-enhanced anisotropic growth. Straight cubic β-Ga_2O_3 NRs with a diameter of 260 nm were obtained, indicating a good crystal quality. XRD, PL, and Raman spectra analyses show that the β-Ga_2O_3 NRs grow along the *a*-axis direction of the β-Ga_2O_3 unit cell and contain arsenic residue. The simulation results demonstrate that the β-Ga_2O_3 NR film exhibits strong light-matter interaction at different structural periods, incident angles, and wavelengths. The experimental optical reflectance spectrum indicates that the reflectance of the β-Ga_2O_3 NR film at a wavelength of 254 nm is only 0.05, which is 40 % lower than that of β-Ga_2O_3 thin film. These findings suggest that the β-Ga_2O_3 NR film is a promising candidate for optoelectronic devices with high light-matter interaction.

Funding

This work was partly supported by the National Key Research and Development Program under Grant 2022YFB3605500 and partly by the

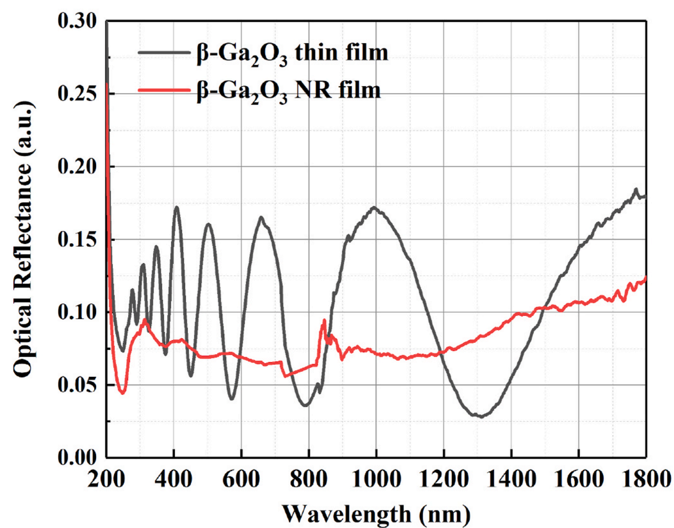

Fig. 10. The measured optical reflectance spectra of β-Ga_2O_3 thin film and NR film.

Natural Science Foundation of Jilin Province under Grant 20230101124JC and 20220101119JC.

CRediT authorship contribution statement

Wei Chen: Writing – review & editing, Writing – original draft, Conceptualization. **Teng Jiao:** Data curation. **Peiran Chen:** Visualization. **Xinming Dang:** Software. **Yu Han:** Validation. **Han Yu:** Formal analysis. **Xin Dong:** Supervision. **Yuantao Zhang:** Methodology. **Baolin Zhang:** Investigation.

Declaration of competing interest

The authors declare that they have no known competing financial interests or personal relationships that could have appeared to influence the work reported in this paper.

Data availability

Data will be made available on request.

Appendix A. Supplementary data

Supplementary data to this article can be found online at https://doi.org/10.1016/j.mssp.2023.107912.

References

[1] D. Guo, Q. Guo, Z. Chen, Z. Wu, W. Tang, Review of Ga_2O_3 based optoelectronic devices, Materials Today Physics 11 (22) (2019), 100157.
[2] J. Zhu, Z. Xu, S. Ha, D. Li, K. Zhang, H. Zhang, J. Feng, Gallium oxide for gas sensor applications: a comprehensive review, Materials 15 (20) (2022) 7339.
[3] S.J. Pearton, J. Yang, P.H. Cary, F. Ren, J. Kim, M.J. Tadjer, M.A. Mastro, A Review of Ga_2O_3 Materials, Processing, and Devices, Amer Inst Physics, MELVILLE, 2018.
[4] X.C. Guo, N.H. Hao, D.Y. Guo, Z.P. Wu, Y.H. An, X.L. Chu, L.H. Li, P.G. Li, M. Lei, W.H. Tang, β-Ga_2O_3/p-Si heterojunction solar-blind ultraviolet photodetector with enhanced photoelectric responsivity, J. Alloys Compd. 660 (2016) 136–140.
[5] I. López, A. Castaldini, A. Cavallini, E. Nogales, B. Méndez, J. Piqueras, β-Ga_2O_3 nanowires for an ultraviolet light selective frequency photodetector, J. Phys. Appl. Phys. 47 (41) (2014).
[6] H.F. Mohamed, C. Xia, Q. Sai, H. Cui, M. Pan, H. Qi, Growth and fundamentals of bulk β-Ga_2O_3 single crystals, J. Semiconduct. 40 (1) (2019), 11801.
[7] A. Kuramata, K. Koshi, S. Watanabe, Y. Yamaoka, T. Masui, S. Yamakoshi, High-quality β-Ga_2O_3 single crystals grown by edge-defined film-fed growth, Jpn. J. Appl. Phys. 55 (12) (2016).
[8] Y. Chen, H. Liang, X. Xia, R. shen, Y. Liu, Y. Luo, G. Du, Effect of growth pressure on the characteristics of β-Ga_2O_3 films grown on GaAs (100) substrates by MOCVD method, Appl. Surf. Sci. 325 (2015) 258–261.
[9] Y. Chen, X. Xia, H. Liang, Q. Abbas, Y. Liu, G. Du, Growth pressure controlled nucleation epitaxy of pure phase ε- and β-Ga_2O_3 films on Al2O3 via metal–organic chemical vapor deposition, Cryst. Growth Des. 18 (2) (2018) 1147–1154.
[10] W. Ding, X. Meng, High performance solar-blind UV detector based on β-Ga_2O_3/GaN nanowires heterojunction, J. Alloys Compd. 866 (2021), 157564.
[11] N. Zhu, K. Ma, P. Zhang, X. Xue, J. Su, Modulated interfacial band alignment of β-Ga_2O_3/GaN heterojunction by the polarization charge transfer, Appl. Surf. Sci. 586 (2022), 152831.
[12] Z.L. Wang, R.P. Gao, Z.W. Pan, Z.R. Dai, Nano-scale mechanics of nanotubes, nanowires, and nanobelts, Adv. Eng. Mater. 3 (9) (2001) 657–661.
[13] A. Afzal, β-Ga_2O_3 nanowires and thin films for metal oxide semiconductor gas sensors: sensing mechanisms and performance enhancement strategies, JOURNAL OF MATERIOMICS 5 (4) (2019) 542–557.
[14] S. Xu, L. Liu, G. Qu, X. Zhang, C. Jia, S. Wu, Y. Ma, Y.J. Lee, G. Wang, J.-H. Park, Y. Zhang, X. Yi, Y. Wang, J. Li, Single β-Ga_2O_3 nanowire based lateral FinFET on Si, Appl. Phys. Lett. 120 (15) (2022).
[15] D. Tham, C.Y. Nam, J.E. Fischer, Defects in GaN nanowires, Adv. Funct. Mater. 16 (9) (2006) 1197–1202.
[16] P. Yang, R. Yan, D. Gargas, Nanowire photonics, Nat. Photonics 3 (10) (2009) 569–576.
[17] M.C. Pedapudi, J.C. Dhar, Ultrasensitive p-n junction UV-C photodetector based on p-Si/beta-Ga_2O_3 nanowire arrays, Sensors and actuators. A. Physical. 344 (2022), 113673.
[18] S.-Y. Chu, M.-J. Wu, T.-H. Yeh, C.-T. Lee, H.-Y. Lee, Investigation of high-sensitivity NO 2 gas sensors with Ga 2 O 3 nanorod sensing membrane grown by hydrothermal synthesis method, Nanomaterials 13 (6) (2023).
[19] M. Cholines Pedapudi, J.C. Dhar, High temperature annealing on vertical p-n junction p-NiO/n-β-Ga_2O_3 nanowire arrays for high performance UV photodetection, Mater. Sci. Semicond. Process. 163 (2023), 107592.
[20] Y. Bayam, V.J. Logeeswaran, A.M. Katzenmeyer, R.B. Sadeghian, R.J. Chacon, M. C. Wong, C.E. Hunt, K. Motomiya, B. Jeyadevan, M.S. Islam, Synthesis of Ga_2O_3 nanorods with ultra-sharp tips for high-performance field emission devices, Sci. Adv. Mater. 7 (2) (2015) 211–218.
[21] W. Ruan, Z. Wu, J. Liu, J. Chen, Y. Shan, P. Song, Z. Jiang, R. Liu, G. Zhang, Z. Fang, β-Ga_2O_3 nanowires: controlled growth, characterization, and deep-ultraviolet photodetection application, J. Phys. Appl. Phys. 55 (28) (2022).
[22] S. Wang, H. Sun, Z. Wang, X. Zeng, G. Ungar, D. Guo, J. Shen, P. Li, A. Liu, C. Li, W. Tang, In situ synthesis of monoclinic β-Ga_2O_3 nanowires on flexible substrate and solar-blind photodetector, J. Alloys Compd. 787 (2019) 133–139.
[23] B. Alhalaili, H. Mao, D.M. Dryden, H. Cansizoglu, R.J. Bunk, R. Vidu, J. Woodall, M. Saif Islam, Influence of silver as a catalyst on the growth of βga_2o_3 nanowires on gaas, Materials 13 (23) (2020) 1–15.
[24] L.S. Reddy, Y.H. Ko, J.S. Yu, Hydrothermal synthesis and photocatalytic property of β-Ga_2O_3 nanorods, Nanoscale Res. Lett. 10 (1) (2015) 364.
[25] W. Chen, T. Jiao, Z. Li, Z. Diao, Z. Li, X. Dong, Y. Zhang, B. Zhang, Preparation of β-Ga_2O_3 nanostructured films by thermal oxidation of GaAs substrate, Ceram. Int. 48 (4) (2022) 5698–5703.
[26] H.W. Kim, N.H. Kim, Growth of gallium oxide thin films on silicon by the metal organic chemical vapor deposition method, Materials science & engineering, B, Solid-state materials for advanced technology 110 (1) (2004) 34–37.
[27] C.B. Alcock, V.P. Itkin, M.K. Horrigan, Vapour pressure equations for the metallic elements: 298-2500K, Can. Metall. Q. 23 (3) (1984) 309–313.
[28] I.W. Yeu, G. Han, C.S. Hwang, J.-H. Choi, An ab initio approach on the asymmetric stacking of GaAs $< 111 >$ nanowires grown by a vapor-solid method, Nanoscale 12 (34) (2020) 17703–17714.
[29] M. Gruart, G.n. Jacopin, B. Daudin, Role of Ga surface diffusion in the elongation mechanism and optical properties of catalyst-free GaN nanowires grown by molecular beam epitaxy, Nano Lett. 19 (7) (2019) 4250–4256.
[30] N.A.K. Kaufmann, L. Lahourcade, B. Hourahine, D. Martin, N. Grandjean, Critical impact of Ehrlich–Schwöbel barrier on GaN surface morphology during homoepitaxial growth, J. Cryst. Growth 433 (2016) 36–42.
[31] Y. Zhang, A.M. Sanchez, Y. Sun, J. Wu, M. Aagesen, S. Huo, D. Kim, P. Jurczak, X. Xu, H. Liu, Influence of droplet size on the growth of self-catalyzed ternary GaAsP nanowires, Nano Lett. 16 (2) (2016) 1237–1243.
[32] V.G. Dubrovskii, N.V. Sibirev, Growth rate of a crystal facet of arbitrary size and growth kinetics of vertical nanowires, Phys. Rev. E: Stat. Phys., Plasmas, Fluids, Relat. Interdiscip. Top. 70 (3) (2004) 1–31604.
[33] C. Kranert, C. Sturm, R. Schmidt-Grund, M. Grundmann, Raman tensor elements of β-Ga_2O_3, Sci. Rep. 6 (1) (2016) 35964, 35964.
[34] Y. Zhu, W. Zheng, W. Wang, S. Zhu, L. Cheng, L. Li, Z. Lin, Y. Ding, M. Jin, F. Huang, Raman tensor of layered black arsenic, J. Raman Spectrosc. 51 (8) (2020) 1324–1330.
[35] M.A. Ochoa, J.E. Maslar, H.S. Bennett, Extracting electron densities in n-type GaAs from Raman spectra: comparisons with Hall measurements, J. Appl. Phys. 128 (7) (2020), 75703.
[36] Y.K. Frodason, K.M. Johansen, L. Vines, J.B. Varley, L.C.A. Lawrence Livermore National Lab, Self-trapped hole and impurity-related broad luminescence in β-Ga_2O_3, J. Appl. Phys. 127 (7) (2020) 75701–75709.
[37] Q.D. Ho, T. Frauenheim, P. Deák, Origin of photoluminescence in β−Ga_2O_3, Phys. Rev. B 97 (11) (2018).